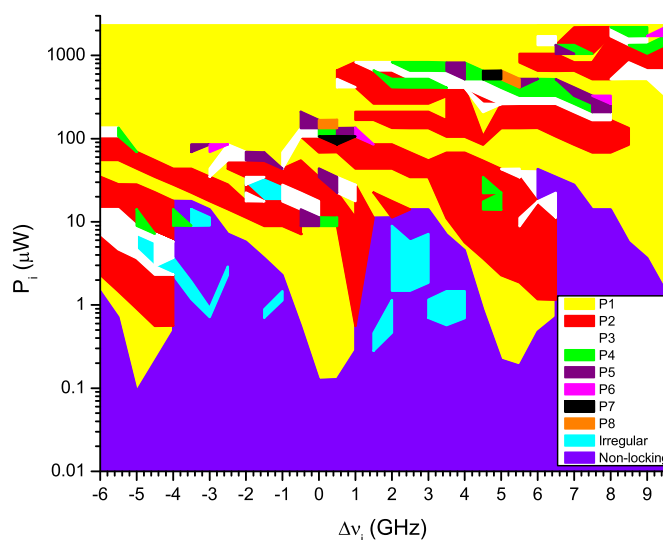


# Nonlinear Dynamics Induced by Optical Injection in Optical Frequency Combs Generated by Gain-Switching of Laser Diodes

Volume 12, Number 4, August 2020

Ana Quirce  
Alejandro Rosado  
Jaime Díez  
Angel Valle  
Antonio Pérez-Serrano  
Jose-Manuel G. Tijero  
Luis Pesquera  
Ignacio Esquivias



DOI: 10.1109/JPHOT.2020.3009450

# Nonlinear Dynamics Induced by Optical Injection in Optical Frequency Combs Generated by Gain-Switching of Laser Diodes

Ana Quirce <sup>1,3</sup>, Alejandro Rosado <sup>2</sup>, Jaime Díez,<sup>1</sup> Angel Valle <sup>1</sup>,  
Antonio Pérez-Serrano <sup>2</sup>, Jose-Manuel G. Tijero <sup>2</sup>,  
Luis Pesquera <sup>1</sup> and Ignacio Esquivias<sup>2</sup>

<sup>1</sup>Instituto de Física de Cantabria, Consejo Superior de Investigaciones Científicas (CSIC)-Universidad de Cantabria, 39005 Santander, Spain

<sup>2</sup>CEMDATIC-E.T.S.I Telecomunicación, Universidad Politécnica de Madrid, 28040 Madrid, Spain

<sup>3</sup>Faculty of Engineering Sciences, Brussels Photonics (B-PHOT), Vrije Universiteit Brussel, 1050 Brussels, Belgium

DOI:10.1109/JPHOT.2020.3009450

This work is licensed under a Creative Commons Attribution 4.0 License. For more information, see <https://creativecommons.org/licenses/by/4.0/>

Manuscript received June 1, 2020; revised July 7, 2020; accepted July 11, 2020. Date of publication July 21, 2020; date of current version July 29, 2020. This work was supported by the Ministerio de Economía y Competitividad of Spain under Grants RTI2018-094118-B-C21 and RTI2018-094118-B-C22, and by Comunidad de Madrid, European Structural Funds (P2018/NMT-4326) and APOYO-JOVENES-KXHJ8C-16-VCKM78. The work of Ana Quirce was supported by the Beatriz Galindo program, Ministerio de Ciencia, Innovación y Universidades (Spain). Corresponding author: Angel Valle (e-mail: valle@ifca.unican.es).

**Abstract:** We present experiments and numerical simulations of optical frequency combs generated by gain-switching a single mode laser diode when subject to optical injection. Our analysis focuses on the combs with a frequency separation  $f_R$  in the GHz range. We present experimental maps in the parameter space spanned by the detuning and the strength of the optical injection that identify the boundaries between regions with different dynamical states. A rich variety of nonlinear behaviors including injection-locked, unlocked and irregular combs are observed and analyzed. The dynamical state corresponding to an injection locked comb,  $PN$ , is characterized by an optical phase oscillation with a well defined amplitude in such a way that repeats or changes in  $2\pi$  with an  $N/f_R$  period, where  $N$  is a natural number. Different regions of locked combs with a tongue shape around detuning values given by multiples of  $f_R$  appear in the maps. P1 and P2 are the most widespread locked states for large values of the modulation amplitude. As this amplitude decreases a much larger variety of  $PN$  states with large values of  $N$  appear in small area regions of the map. Our numerical simulations are in very good agreement with experimental results.

**Index Terms:** Optical frequency combs, gain-switching, laser diode, optical injection, nonlinear dynamics.

## 1. Introduction

Optical frequency combs (OFCs) are coherent light sources consisting of evenly spaced discrete spectral components. From their early applications, mainly in the field of frequency metrology and high accuracy spectroscopy [1], OFCs have also been used in optical ranging [2], high-speed

optical communications [3]–[5], optical arbitrary waveform generation [6] and gas-sensing [7], [8]. One possibility for generating OFCs is to use semiconductor lasers due to their acknowledged advantages: high efficiency, small footprint, and low cost. Four different approaches have been used to generate OFCs in laser diodes: mode-locking [9], electro-optic modulation [10], micro-ring resonators [11], and gain switching (GS) [12].

Gain switching technique consist in driving the semiconductor laser by a radio-frequency (RF) current, typically sinusoidal, superimposed to a direct bias current. From the early demonstration of OFC generation by GS [12], [13] considerable attention has been paid to this technique [4], [5], [14]–[24]. Additional advantages of the technique are flexibility in the selection of the frequency spacing, low losses, compactness, low energy consumption, and easy implementation [12]. Applications of OFCs generated by GS include radio-over-fiber [5] and multi-carrier optical communications [3], [4], [25], absorption spectroscopy [20], [21], and sub-THz generation [26]. The key parameters determining the temporal and spectral characteristics of the generated OFCs are the amplitude and frequency of the RF current together with the bias current applied to the laser diode. Experimental analysis of key issues for OFCs applications, like phase noise/linewidth, frequency span, jitter, and frequency chirp, have been recently performed [14], [22], [27], [28]. These issues also have been analyzed from a theoretical point of view using rate equations-based numerical models [15]–[17]. Very recently a systematic experimental and simulation analysis of the effect of the driving conditions on the OFCs characteristics has been performed [24].

External optical injection (OI) in semiconductor lasers has also been a subject of interest for many years [29], [30]. OI in continuous wave (CW) single-mode lasers induces a wide variety of nonlinear dynamical regimes, including injection locking, four-wave mixing, and periodic and chaotic behaviours [30]. Injection locking improves the laser emission characteristics by reducing the frequency chirp and noise, and by enhancing the intrinsic frequency response [30]. Injection of OFC into a single-mode CW slave laser has received recently a lot of attention [31]–[35]. As the slave's frequency is detuned by a rational fraction of the injected OFC spacing, it becomes frequency locked [31]. These locked states are more commonly known as Arnol'd tongues.

The complementary situation, in which light from a CW laser is injected in gain-switched lasers, has also been analyzed. In this case OI improves the spectral characteristics of the OFCs when performed under specific injection conditions. For instance, OI can transform a broad noisy optical spectrum from a sinusoidally GS single-mode laser into a high quality OFC [12]. This transformation has been demonstrated to be particularly dramatic for pulsed GS lasers for which broad OFCs with small line separations (smaller than 500 MHz) were experimentally obtained [23]. Another advantage of injection locking in GS lasers is that a significant reduction of the linewidth of individual comb lines can be obtained by using a narrow linewidth CW master laser (ML), because the low linewidth of the ML is transferred to the OFC lines [17], [22], [27]. Numerical simulations also show that the locking range for GS lasers is considerable greater than that corresponding to CW lasers because the OFC can be locked by injecting close to one of the central lines of the comb [17]. Detrimental characteristics like time jitter, phase noise and relative intensity noise (RIN) can also be reduced by appropriate external OI [12], [14], [16], [36], [37]. In fact theoretical analysis show that reduction of the pulse-to-pulse phase noise, time jitter and RIN causes a large increase of the carrier-to-noise ratio (CNR), as well as a decrease of the linewidth of each comb line [16].

In a recent work we have performed a systematic analysis of the OI conditions for improving the spectral quality of a GS single-mode laser showing a broad noisy spectrum without injection [24]. This theoretical and experimental analysis mainly focused on the 10 dB spectral width and the CNR, that are two of the most important parameters for characterizing the quality of an OFC. However, a systematic analysis on how OI conditions affect the nonlinear dynamics of the GS laser has not been reported yet.

In this paper we perform that analysis for the first time to the best of our knowledge. This is done by using numerical simulations and experiments on a gain-switched single-mode laser subject to external optical injection. Contrary to [24] we focus on the effect of OI on a good quality OFC. The OFC generator is a single-mode semiconductor laser, which is driven in GS operation

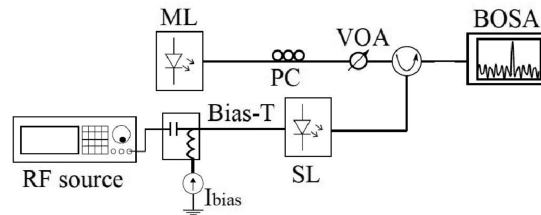


Fig. 1. Experimental setup for performing optical injection in GS operation. SL: slave laser, ML: master laser, PC: polarization controller, VOA: variable optical attenuator, and BOSA: Brillouin optical spectrum analyzer.

using a bias current and a sinusoidal signal with a frequency  $f_R$  in the GHz range. We perform a first experimental measurement of maps, in the injected power-frequency detuning plane, in which we observe injection-locked, non-locked and irregular combs regions. We perform numerical simulations of the system by using the model of [24]. We find different types of locked combs characterized by a frequency spacing equal to rational fractions of  $f_R$ . We term  $PN$  the dynamical state corresponding to a locked comb with  $f_R/N$  frequency separation between consecutive lines of the optical spectrum, where  $N$  is a natural number. The good agreement found between the simulations and the experimental results permits us to characterize the  $PN$  state also by its phase locking behavior: optical phase oscillates with a well defined amplitude in such a way that repeats or changes in  $2\pi$  with an  $N/f_R$  period. Our experimental maps show that  $P1$  and  $P2$  are the most widespread locked states for large values of the modulation amplitude. When decreasing this amplitude a much larger variety of  $PN$  states appear in small area regions of the map.  $PN$  states with large values of  $N$ , up to  $N = 14$ , are observed for the first time, as far as we know. Locking range of combs is much larger than that of CW lasers for which there is only a single locking range, in agreement with previously reported simulations [17]. The presented locking scenarios can be used to generate optical combs with different frequency spacing values.

## 2. Experimental Techniques

Experimentally we attain GS of a laser diode, with or without OI, by using the setup shown in Fig. 1. The laser is a high-bandwidth 1550 nm discrete mode laser (DML) (Eblana Photonics EP1550-0-DM-H19-FM). This is a multi-quantum well device in a ridge waveguide with index perturbations, in order to allow single-mode operation [38]. The threshold current of this laser is  $I_{th} = 14$  mA and its nominal modulation bandwidth is 10 GHz. More details can be found in [24]. The CW bias current,  $I_{bias}$ , and the temperature of the laser were controlled with a laser driver and a temperature controller (Luzwavelabs LDC/E-Current200 and LDC/E-Temp3), respectively. The temperature of the device was held constant at 25 °C. In all the experiments we have used a bias current,  $I_{bias} = 30$  mA, for which the relaxation oscillation frequency,  $\nu_{ROF}$ , is approximately 6 GHz. In order to achieve GS operation the laser was driven by a superposition of  $I_{bias}$  and a sinusoidal modulation current at a frequency  $f_R = 5$  GHz provided by a microwave/RF generator (Keysight N5173B).

Light from a tunable master laser (ML) (Pure Photonics PPCL300), with a narrow linewidth (75 kHz), was injected into the DML, operating as a slave laser (SL), by using an optical circulator. A polarization controller (PC) was used for maximizing the power injected into the SL. The level of injected power into the SL was controlled by using a variable optical attenuator (VOA). The optical injection was characterized by its strength given by the value of the power measured in front of the SL,  $P_i$ , and by its optical frequency,  $\nu_j$ . The output of the SL is spectrally characterized with a high-resolution (10 MHz) Brillouin optical spectrum analyser (BOSA) (Aragon Photonics BOSA 210). The quality of OFCs was characterized by means of the 10 dB spectral width ( $\Delta f_{10}$ ) and the average carrier-to-noise ratio (CNR) of the lines within  $\Delta f_{10}$  [22].

### 3. Theoretical Model

The dynamics of a single-mode semiconductor laser subject to external optical injection can be modelled by using the following set of rate-equations [24], [39]:

$$\frac{dN}{dt} = \frac{I(t)}{eV_{act}} - R(N) - \frac{v_g g(N)S}{1 + \epsilon S} \quad (1)$$

$$\frac{dS}{dt} = \left[ \frac{\Gamma v_g g(N)}{1 + \epsilon S} - \frac{1}{\tau_p} \right] S + 2k_c \sqrt{S S_i} \cos \Phi + \beta \Gamma B N^2 + \sqrt{2\beta \Gamma B N^2 S} F_S(t) \quad (2)$$

$$\frac{d\Phi}{dt} = \frac{\alpha}{2} \left[ \Gamma v_g g(N) - \frac{1}{\tau_p} \right] - 2\pi(\Delta \nu_i + \Delta \nu) - k_c \sqrt{\frac{S_i}{S}} \sin \Phi + \sqrt{\frac{\beta \Gamma B N^2}{2S}} F_\Phi(t) \quad (3)$$

where  $N(t)$  is the carrier density,  $S(t)$  the photon density and  $\Phi(t)$  the optical phase in the reference frame of the master laser, so the electrical field is  $E(t) = \sqrt{S(t)}e^{j(2\pi\nu_i t + \Phi(t))}$ , where  $\nu_i$  is the frequency of the master laser. In these equations  $I(t)$  is the injected current,  $V_{act}$  the active volume,  $e$  the electron charge,  $R(N)$  the carrier recombination rate,  $v_g$  the group velocity,  $g(N)$  the material gain,  $\epsilon$  the non-linear gain coefficient,  $\Gamma$  the optical confinement factor,  $\tau_p$  the photon lifetime,  $\beta$  the fraction of spontaneous emission coupled into the lasing mode and  $\alpha$  the linewidth enhancement factor. The carrier recombination is  $R(N) = AN + BN^2 + CN^3$ , where  $A$ ,  $B$  and  $C$  are the non-radiative, spontaneous, and Auger recombination coefficients, respectively. The material gain  $g(N)$  is given by  $g(N) = \frac{dg}{dN}(N - N_{tr})$ , where  $\frac{dg}{dN}$  is the differential gain and  $N_{tr}$  the transparency carrier density. Neglecting high-frequency electrical effects, the injected current  $I(t)$  is given by:

$$I(t) = I_{bias} + C_{loss}(f_R) \frac{2\sqrt{2}V_{RF}}{Z_0 + Z_l} \sin(2\pi f_R t), \quad (4)$$

where  $V_{RF}$  is the root-mean-square (RMS) voltage of the signal generator applied to an ideal  $50 \Omega$  load,  $C_{loss}(f_R)$  is a loss coefficient accounting for the frequency dependent electrical cable attenuation,  $Z_0$  is the generator output impedance, and  $Z_l$  the impedance of the laser module. The output power coupled to the fiber is given by

$$P(t) = S(t) \frac{\eta_f h c V_{act}}{\lambda_{cw} \Gamma \tau_p} \quad (5)$$

where  $\eta_f$  is the in-fiber external quantum efficiency,  $\lambda_{cw}$  is the CW wavelength, and  $h$  is the Planck constant. The Langevin terms  $F_S(t)$  and  $F_\Phi(t)$  in Eqs. (2)–(3), represent fluctuations due to spontaneous emission, with the following correlation properties,  $\langle F_i(t)F_j(t') \rangle = 2\delta_{ij}\delta(t - t')$ , where  $\delta(t)$  is the Dirac delta function and  $\delta_{ij}$  the Kronecker delta function with the subindexes  $i$  and  $j$  referring to the variables  $S$  and  $\Phi$ .

Terms describing the external optical injection appear in Eq. (2) and Eq. (3). In these terms  $k_c$  is the master-slave coupling coefficient, and  $S_i$  is the photon density of the injected laser field.  $S_i$  is obtained from the power injected by the ML,  $P_i$ , using an expression similar to Eq. (5). Two frequency terms appear in these equations. The first one is the frequency detuning between the ML and the free-running SL when operated in CW at  $I_{bias}$ ,  $\Delta \nu_i = \nu_i - \nu_{cw} = \nu_i - c/\lambda_{cw}$ , where  $\nu_{cw}$  is the frequency corresponding to  $\lambda_{cw}$ , and  $c$  is the speed of light in vacuum. The second frequency term in Eq. (3),  $\Delta \nu$ , is the frequency detuning between  $\nu_{cw}$  and the frequency of the free-running SL at threshold  $\nu_{th}$ ,  $\Delta \nu = \nu_{cw} - \nu_{th}$ . This is a non-vanishing term due to the gain saturation effect. When Eq. (3) is considered for the free-running SL at  $I_{bias}$  it gives

$$\Delta \nu = \nu_{cw} - \nu_{th} = \frac{1}{2\pi} \frac{\alpha}{2} \left( \Gamma v_g g(N) - \frac{1}{\tau_p} \right) \quad (6)$$

This detuning can be evaluated in terms of  $I_{bias}$ ,  $I_{th}$ , and the nonlinear gain coefficient,  $\epsilon$ , as follows. Solving the deterministic version of Eqs. (1), (2) in the steady state with  $\kappa_c = 0$ , and neglecting noise terms ( $\beta = 0$ ), we find for the photon density at  $I_{bias}$ ,  $S_0 = (I_{bias}/(eV_{act}) - R(N_{th}))\Gamma\tau_p$ , where  $N_{th}$  is the threshold carrier density. Applying  $I_{th} = R(N_{th})eV_{act}$  we get  $S_0 = (I_{bias} - I_{th})\Gamma\tau_p/(eV_{act})$ . The

TABLE 1  
Simulation Parameters

Symbol	Laser values	Units
$V_{act}$	$1.53 \times 10^{-17}$	$\text{m}^3$
$\Gamma$	0.06	-
$N_{tr}$	$1.23 \times 10^{24}$	$\text{m}^{-3}$
$B$	$1.5 \times 10^{-16}$	$\text{m}^3\text{s}^{-1}$
$\frac{dg}{dN}$	$4.38 \times 10^{-20}$	$\text{m}^2$
$n_g$	3.5	-
$\tau_p$	$2.17 \times 10^{-12}$	s
$A$	$2.8 \times 10^8$	$\text{s}^{-1}$
$C$	$9.0 \times 10^{-41}$	$\text{m}^6\text{s}^{-1}$
$\beta$	$5.3 \times 10^{-6}$	-
$\epsilon$	$1.97 \times 10^{-23}$	$\text{m}^3$
$\alpha$	3	-
$Z_0$	50	$\Omega$
$Z_l$	50	$\Omega$
$C_{loss}$ (at 5 GHz)	0.7	-
$\eta_f$	0.17	-

substitution in Eq. (6) of the relation obtained from  $\dot{S} = 0$ ,  $\Gamma v_g g(N) = (1 + \epsilon S_0)/\tau_p$ , and the previous expression for  $S_0$  gives

$$\Delta\nu = \frac{\alpha\epsilon\Gamma(l_{bias} - l_{th})}{4\pi eV_{act}} \quad (7)$$

If we use  $\Delta\nu$  given by Eq. (7),  $\dot{\Phi}$  for the SL at  $l_{bias}$  satisfies  $\dot{\Phi} = -2\pi\Delta\nu_j$  and then,  $\Phi(t) = -2\pi\Delta\nu_j t + \Phi_0$ , where  $\Phi_0$  is constant. Therefore,  $E(t) = \sqrt{S_0} e^{i(2\pi\nu_{cw}t + \Phi_0)}$ , as required. In the same way, for injection locked CW laser we impose  $\dot{N} = \dot{S} = \dot{\Phi} = 0$ . This means that  $\Phi$  is constant and the laser emits at  $\nu_j$ , as expected.

We have used the laser parameters [24] that were extracted for a laser similar to that used in our experiments. The main differences with our laser are that the threshold current was 14.8 mA instead of  $l_{th} = 14$  mA, and that the emission wavelengths are slightly different. We show the laser parameters in Table 1. In order to calculate the optical spectrum we integrate Eqs. (1)–(3) using a 0.01 ps integration time step. We have checked that with this integration time step the photon density is always positive. Fast Fourier transform of the optical field written in the reference frame of the emission frequency of the slave laser operating in CW without optical injection,  $\mathcal{E}(t) = \sqrt{P(t)} e^{i(2\pi\Delta\nu_j t + \Phi(t))}$ , are performed using a 2.5 ps sampling time and a 40.96 ns temporal window. Optical spectra are calculated by averaging over 20 temporal windows.

#### 4. Results and Discussion

We first discuss the results obtained without optical injection. We consider driving conditions leading to a high quality OFC: a modulation voltage  $V_{RF} = 1$  V, repetition frequency  $f_R = 5$  GHz, and  $l_{bias} = 30$  mA [24]. In this case the coherence of the pulses emitted by the free-running gain-switched SL is maintained because the laser is not completely switched-off between pulses [16], [24]. Fig. 2(a) shows the experimental optical spectrum. The frequency separation between consecutive lines is 5 GHz, that approximately corresponds to 0.04 nm wavelength separation. This

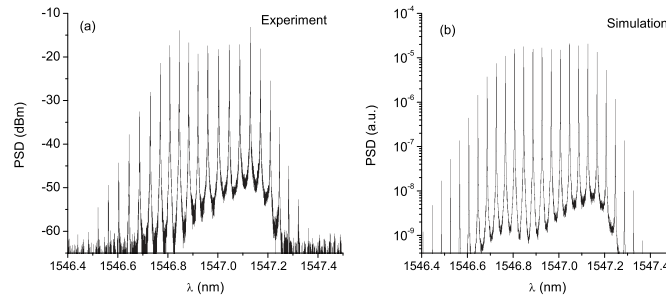


Fig. 2. Experimental (a) and simulated (b) optical spectra (PSD: Power Spectral Density) of the gain-switched laser ( $I_{bias} = 30$  mA,  $f_R = 5$  GHz, and  $V_{RF} = 1$  V) without optical injection.

spectrum shows a high value of CNR ( $> 35$  dB) and a spectral width  $\Delta f_{10} > 50$  GHz. The optical spectrum of the SL in CW operation shows a well defined line at 1546.985 nm wavelength. As  $V_{RF}$  is increased, this comb line moves towards a longer wavelength and new comb lines begin to appear due to the modulation of the bias current. For conditions corresponding to Fig. 2(a) the CW line has shifted to 1547.005 nm. This redshift is due to the temperature increase caused by the sinusoidal excitation of the bias current in comparison with the constant value corresponding to CW operation. In our simulations this redshift does not appear because our model does not consider thermal effects. Therefore we consider in our calculations  $\lambda_{cw} = 1547.005$  nm for obtaining the best comparison between experimental and simulation results. The theoretical optical spectrum corresponding to Fig. 2(a) is shown in Fig. 2(b). Both spectra are very similar, in terms of shape, flatness, CNR and width, the main difference being the absence of the BOSA background noise, which has not been taken into account in our simulations.

From now on we will analyze, using experiments and simulations, the effect of optical injection on the respective OFCs. We first analyze how the OFCs obtained with a large modulation voltage, like those of Fig. 2, change when applying OI. In order to compare between experimental and simulation results we have to estimate the master-slave coupling coefficient,  $k_c$ . This is done by fixing a value of  $\Delta\nu_j$  and searching for the value of  $k_c$  for which the minimum injected power required to achieve locking of the slave OFC to the master laser equals the experimental value. When following this procedure for  $\Delta\nu_j = -2$  GHz we obtain  $k_c = 5.5 \times 10^{10} \text{ s}^{-1}$ , which is similar to the value obtained in [24] for a similar device in a similar set-up.

We show in Fig. 3 experimental and simulated OFCs obtained when the injected power,  $P_i$ , is increased for a fixed value of the detuning,  $\Delta\nu_j = -2$  GHz. In this way we illustrate the effect of OI on the high quality OFC shown in Fig. 2.

When  $P_i$  is very small the optical spectrum is mainly composed of two OFCs with the same frequency spacing  $f_R$ , as it is shown in Fig. 3(a) and (f). The most intense OFC is very similar to that corresponding to the GS free-running SL. The second OFC is due to the injected master field because its lines appear at wavelengths  $\lambda_j + n \times 0.04$  nm (with  $n$  being an integer). Four wave mixing (FWM) components also appear due to the beating between a line from the SL OFC and the closest frequency from the modulated fields of the injected laser. The presence of FWM terms indicates the absence of locking. As  $P_i$  is increased, the SL OFC begins to undergo some frequency pulling (see Fig. 3(b) and (g)) and eventually the slave comb locks to the master laser (see Fig. 3(c) and (h)). These last spectra are centered at  $\lambda_j$  with a frequency spacing of  $f_R$ . We denote the dynamic state corresponding to these spectra as P1. Fig. 3(a)–(c) experimentally confirm the transition to P1 that was first theoretically described in [17]. When  $P_i$  is further increased combs centered at  $\lambda_j$  with a frequency spacing equal to rational fractions of the repetition frequency,  $f_R/N$  ( $N$  being a natural number), are obtained. We denote these dynamical regimes as PN because the temporal trace of the output power has a period given by  $N/f_R$ . An example of OFCs corresponding to P2 is shown in Fig. 3(d) and (i). Further increase of  $P_i$  leads again to P1 dynamics (see Fig. 3(e) and (j)) in which CNR has increased and  $\Delta f_{10}$  has decreased. Fig. 3 shows that there is a very good agreement between simulations and experiments.

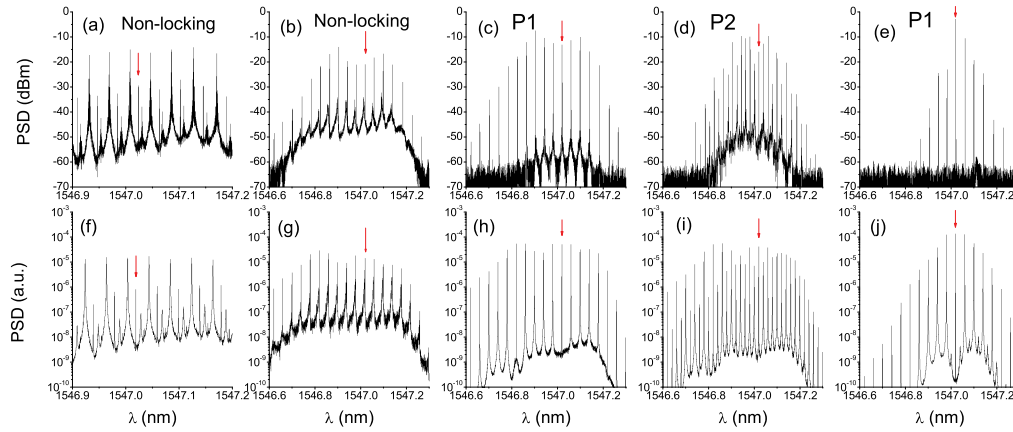


Fig. 3. Experimental (upper row) and simulated (lower row) optical spectra of the gain-switched laser ( $I_{bias} = 30$  mA,  $f_R = 5$  GHz, and  $V_{RF} = 1$  V) with optical injection at detuning  $\Delta\nu_i = -2$  GHz and different values of injected power  $P_i$ , (a), (f) 41 nW, (b), (g) 1.9  $\mu$ W, (c), (h) 3.67  $\mu$ W, (d), (i) 14  $\mu$ W, and (e), (j) 415.4  $\mu$ W. The injection frequency is indicated with an arrow.

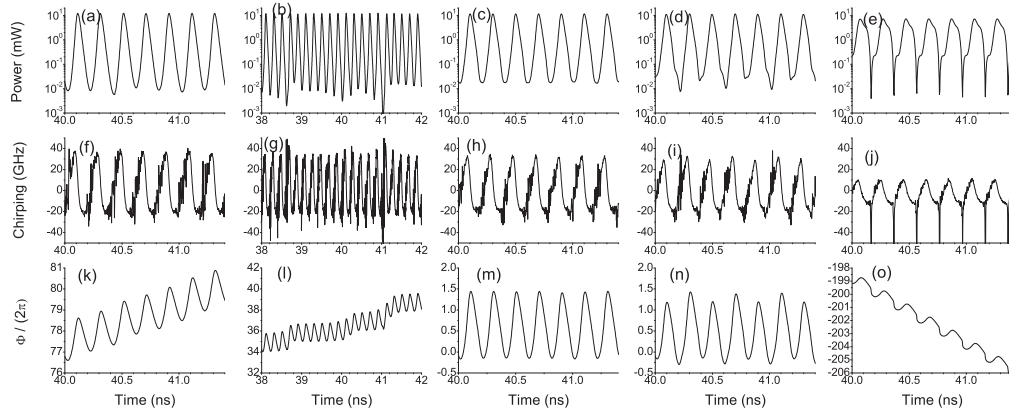


Fig. 4. Simulated power (upper row), frequency chirping (middle row) and optical phase (lower row) of the gain-switched SL ( $I_{bias} = 30$  mA,  $f_R = 5$  GHz, and  $V_{RF} = 1$  V) with optical injection at detuning  $\Delta\nu_i = -2$  GHz and different values of injected power  $P_i$ , (a), (f), (k) 41 nW, (b), (g), (l) 1.9  $\mu$ W, (c), (h), (m) 3.67  $\mu$ W, (d), (i), (n) 14  $\mu$ W, (e), (j), (o) 415.4  $\mu$ W.

That similarity indicates that the analysis of the internal variables can be used for a better understanding of the effect of the OI on the OFC dynamics. We show in Fig. 4 the simulated temporal profiles of the output power, the frequency chirp,  $\frac{1}{2\pi} \frac{d\phi}{dt}$ , and the optical phase,  $\Phi(t)$ , corresponding to Fig. 3. We have plotted the chirp because it plays a double role: on one hand, it gives a good idea on the evolution of the carrier density [24] and on the other hand, it helps to understand the evolution of the optical phase.

Fig. 4(a) shows that the optical power for a very low value of  $P_i$  is almost deterministic: in fact, minimum values of power are well above the power level where the fluctuations due to spontaneous emission dominate the evolution (around  $10^{-7}$  mW). Power, chirping (Fig. 4(f)) and phase (Fig. 4(k)) are very similar to those corresponding to an OFC without OI [24].  $\Phi$  oscillates around a value that increases linearly with time with a slope given by  $-2\pi \Delta\nu_i$  because the OFC is centered at  $\nu_{CW}$  and  $\Phi$  is defined in the OI reference frame. The evolution of  $\Phi$  shown in Fig. 4(l) and (m) illustrates the transition to locked OFC. Fig. 4(l) shows that just before locking, the increase shown

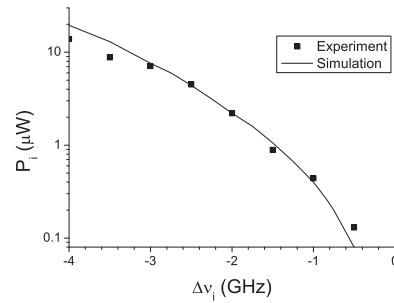


Fig. 5. Experimental (squares) and simulated (solid line) injected power necessary to get P1 dynamical regime as a function of the frequency detuning. In this figure  $I_{bias} = 30$  mA,  $f_R = 5$  GHz, and  $V_{RF} = 1$  V.

in Fig. 4(k) disappears because there are regions in which  $\Phi$  oscillates around a constant value with random duration. When the OFC locks to OI (Fig. 4(m)),  $\Phi$  maintains its oscillation around a constant value for all times. P1 state is also characterized by smaller power fluctuations (compare Fig. 4(c) and (a)), smaller chirping fluctuations (compare Fig. 4(h) and (f)), and smaller fluctuations in the amplitude of phase oscillations. Smaller fluctuations due to locking explain that the spectra corresponding to P1 have higher CNR than those corresponding to free-running OFCs (compare Figs. 3(h) and 2(b)). However  $\Delta f_{10}$  in these spectra are similar because the frequency chirping and the Full Width at Half Maximum (FWHM) of optical power pulses for locked and free-running OFCs are similar (around 50 GHz and 32 ps, respectively). Fig. 4(d), (i) and (n) illustrate the dynamics for P2 regime corresponding to Fig 3(i). Phase and power traces show a clear repetition each  $2/f_R$ .  $\Phi$  is a bounded quantity, as it was for P1 regime in Fig. 4(m), because frequency chirping excursions around zero value are symmetric (in the sense that the area above zero chirping equals to the area below). However the bounded character of  $\Phi$  is not always maintained for locked OFCs. As  $P_i$  is increased  $\Phi$  oscillates around a value that decreases linearly with time with  $2\pi f_R$  slope, as it is illustrated in Fig. 4(o). Nevertheless the periodic character of the phase is maintained in a reference system centered at  $\nu_i - f_R$  (instead of  $\nu_i$ ) since  $\Phi$  decreases  $2\pi$  after each period.  $\Phi$  decreases with time because chirping is no longer symmetric around zero, taking mostly negative values. Chirping excursions decrease [40], becoming smaller than those of previous cases, while the FWHM of the pulses increases (64 ps in Fig. 4(e)). In this way  $\Delta f_{10}$  decreases when  $P_i$  increases, as it can be observed in the experimental results shown in Fig. 3(e).

The main difference between the evolution of the optical phase in non-locked and locked OFCs becomes apparent when the evolution of the phase is analyzed in the reference frame of the SL at CW operation,  $\phi_{cw}$ , instead of  $\Phi$ , for the case of Fig. 4(k). For unlocked OFCs  $\phi_{cw}$  also oscillates with similar amplitudes to those of Fig. 4(m) but the value around which oscillation occurs performs a Brownian motion that becomes apparent in a longer time scale ( $\mu\text{s}$ ) than that considered in Fig. 4. Also fluctuations in the amplitudes of  $\phi_{cw}$  are much larger than those observed in Fig. 4(m). Phase behavior of the unlocked case of Fig. 4(k) is very similar to that observed for free-running OFCs. This was analyzed in [16] by assuming that the phase remains constant over the duration of the pulse and only varies from pulse to pulse. Our results are in agreement with those obtained with the assumption of a pulse-to-pulse phase performing a Brownian evolution while preserving some memory of the phase of the preceding pulses [16]. In contrast with free-running OFCs, when locked OFCs are considered  $\Phi$  oscillates with a well defined amplitude around a constant value (see Fig. 4(m)), or around a value that changes linearly with time with a  $2\pi$  phase change in each period (see Fig. 4(o)).

We characterize now the transition to P1 as a function of the frequency detuning. Fig. 5 shows experimental and simulation values of the minimum  $P_i$  required to achieve locking of the SL OFC to the ML. Experimentally this is done by fixing  $\Delta\nu_i$  and searching for the value of  $P_i$  for which we first get a spectrum similar to that of Fig. 3(c). Theoretically we look for the  $P_i$  value for which we first get a bounded  $\Phi$  similar to that of Fig. 4(m). Good agreement is found between experimental

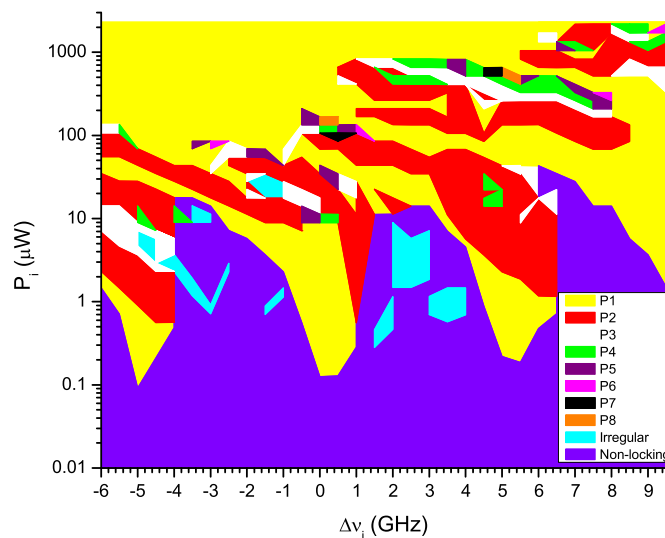


Fig. 6. Experimental values of the injected power as a function of the frequency detuning at which different dynamical regimes are observed for  $I_{bias} = 30$  mA,  $f_R = 5$  GHz, and  $V_{RF} = 1$  V.

and theoretical results. Experimental results show that  $\sqrt{P_i}$  decreases linearly with  $\Delta\nu_i$ : a linear fit gives  $\sqrt{P_i} = -0.995\Delta\nu_i - 0.362$ , with  $R^2 = 0.992$ . This dependence coincides with that theoretically found for the saddle-node bifurcation that appears in CW lasers subject to OI [30]. However we note that the  $P_i$  required to lock an OFC is significantly smaller than that needed to lock a CW laser: for instance, for  $\Delta\nu_i = -2$  GHz, the CW laser locks when  $P_i = 6\mu\text{W}$  while the OFC locks when  $P_i = 2.2\mu\text{W}$ .

We now present experimental maps in the  $P_i$  vs  $\Delta\nu_i$  plane identifying the boundaries between regions with different nonlinear dynamics. We show in Fig. 6 the map obtained for  $I_{bias} = 30$  mA, and  $V_{RF} = 1$  V. The map is obtained by fixing  $\Delta\nu_i$  and increasing  $P_i$  by using the variable attenuator, without switching-off the ML. We obtain different dynamical behaviours including PN, unlocked, and irregular dynamics. We consider that a PN regime occurs when there are comb lines with an amplitude greater than 25 dB with respect to the noise level and this ratio is greater than 10 dB for some comb lines separated by  $f_R/N$ . Irregular dynamics is characterized by low values of the ratio between the intensity of comb lines and noise level. We consider that this irregular behaviour occurs when this ratio is smaller or equal than 25 dB for all comb lines. Other unlocked regions are labelled as Non-locking in Fig. 6.

The minimum injected power required to achieve P1 has local minima for detunings given by  $nf_R$ , i.e. injecting close to one of the comb lines. We obtain several regions of locked combs with a tongue shape around detuning values given by multiples of  $f_R$ . Map displays a clear asymmetry between negative and positive detuning regions. This asymmetry is due to the amplitude-phase coupling. For large values of  $P_i$ , P1 dynamics prevails when  $\Delta\nu_i$  is negative, while a much larger variety of PN regimes is observed when  $\Delta\nu_i$  is positive. Importantly, P1 is observed over a very wide  $\Delta\nu_i$  range, much larger than that observed for CW lasers under OI [30], in agreement with previous numerical simulations [17]. Then, an extended locking range is obtained showing that the locking capabilities of gain-switched lasers are higher than those of CW lasers where only a single locking range exists, provided that a different longitudinal mode is not excited.

Fig. 6 shows that P1 and P2 are the most widespread locked OFCs dynamics in the map. PN regions tend to appear as structures of Arnol'd tongue type. These structures can appear when periodically driven nonlinear oscillators are considered. They have been recently observed when an OFC is injected into a single-mode CW slave laser at detunings corresponding to rational fractions of  $f_R$  [31], [32]. This system is complementary to ours because the periodic forcing appears in the

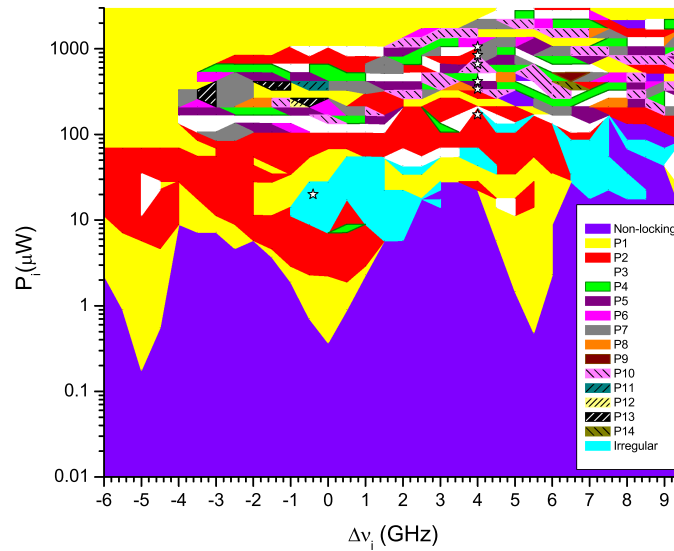


Fig. 7. Experimental values of the injected power as a function of the frequency detuning at which different dynamical regimes are observed for  $I_{bias} = 30$  mA,  $f_R = 5$  GHz, and  $V_{RF} = 0.5$  V. White stars correspond to cases illustrated in Figs. 8 and 10.

electrical field equation while in our case that forcing appears in the carrier density equation. So in our case Arnol'd tongues can appear when the frequency detuning becomes resonant with a rational fraction of  $f_R$  and the OFC becomes frequency locked.

We also show in Fig. 7 the map obtained under the same conditions of Fig. 6 but decreasing the amplitude of the modulation,  $V_{RF}$  to 0.5 V. In this case the simulated optical spectrum without optical injection shows  $CNR = 47$  dB and  $\Delta f_{10} = 35$  GHz. Although some of the main features are similar to those of Fig. 6, we observe many more PN regions with higher values of  $N$ , and with smaller areas. We observe a larger variety of PN states when fixing a  $\Delta v_i$  value and increasing the  $P_i$  value, specially for positive values of the detuning. Dynamics is more complex than in Fig. 6 because the smaller value of  $V_{RF}$  causes a larger impact of the OI on the dynamical evolution. The level of complexity in the dynamics of a CW single-mode semiconductor laser when subject to optical injection [30] is much larger than that corresponding to a single-mode gain-switched laser without optical injection [41]. This is the reason why as  $V_{RF}$  decreases the dynamics of our system becomes more similar to the optically injected laser diode case, and therefore more complex dynamics can be expected.

We now discuss the evolution of the dynamical variables for PN states with large values of  $N$  for which a detailed comparison with simulations is desirable. In order to do this comparison we need to change the value of  $\kappa_c$  because Figs. 6 and 7 were obtained in different experiments to those discussed in Figs. 3 and 5. Values of optical power injected in the SL in experiments corresponding to Figs. 6 and 7 were smaller than those of Figs. 3 and 5 because light was more efficiently coupled in the SL in the experiments of Figs. 3 and 5. This can also be seen in the slight vertical shift downwards of the curve of Fig. 5 when compared to the corresponding curve in Fig. 6. For the case of  $V_{RF} = 0.5$  V, we obtain that  $\kappa_c = 1.5 \times 10^{11} \text{ s}^{-1}$  when comparing experimental and simulated  $P_i$  needed to achieve locked OFCs at  $\Delta v_i = -2$  GHz. We show in Fig. 8(a)–(f) experimental optical spectra obtained when increasing  $P_i$  for  $\Delta v_i = 4$  GHz. These spectra correspond to the following sequence of PN states: P2, P5, P3, P10, P7, and P6. These cases are indicated with white stars in Fig. 7. PN spectra show a clear frequency locking because comb lines appear at  $\nu_i + n f_R / N$ , where  $n$  is an integer. We compare also the P2, P5, and P3 cases with the simulated spectra for similar values of  $P_i$ , shown in the last row of Fig. 8. We obtain a good agreement that permits us to explore the dynamical evolution of optical power, chirping and optical phase, that we show in Fig. 9.

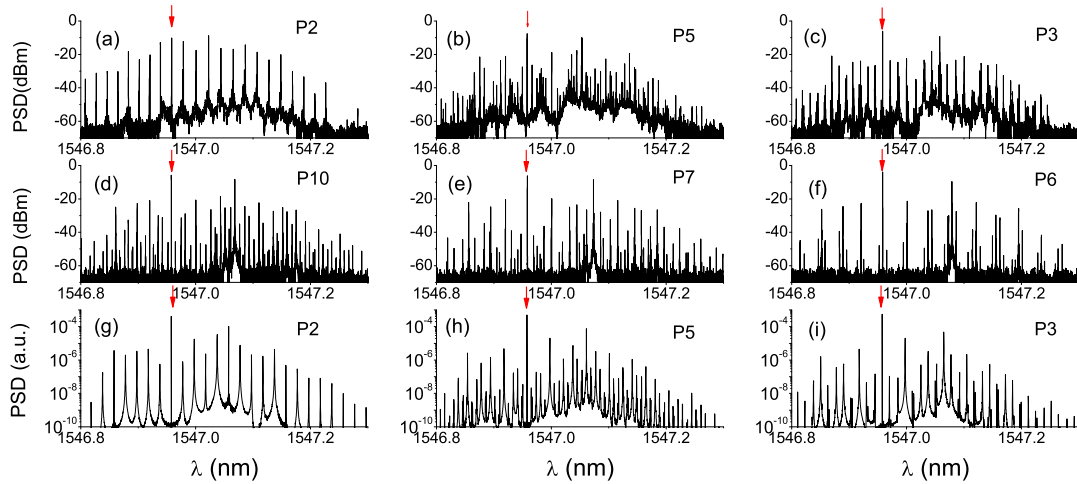


Fig. 8. Experimental (a–f) and simulated (g–i) optical spectra for  $I_{bias} = 30$  mA,  $f_R = 5$  GHz, and  $V_{RF} = 0.5$  V with detuning  $\Delta\nu_i = 4$  GHz and different values of injected power  $P_i$ . Experimental spectra correspond to  $P_i$  values of (a)  $170 \mu\text{W}$ , (b)  $331 \mu\text{W}$ , (c)  $416 \mu\text{W}$ , (d)  $663 \mu\text{W}$ , (e)  $838 \mu\text{W}$ , and (f)  $1060 \mu\text{W}$ . Simulated spectra correspond to  $P_i$  values of (g)  $250 \mu\text{W}$ , (h)  $338 \mu\text{W}$ , and (i)  $416 \mu\text{W}$ . The injection wavelength is indicated with an arrow. In this figure  $\kappa_c = 1.5 \times 10^{11} \text{s}^{-1}$ .

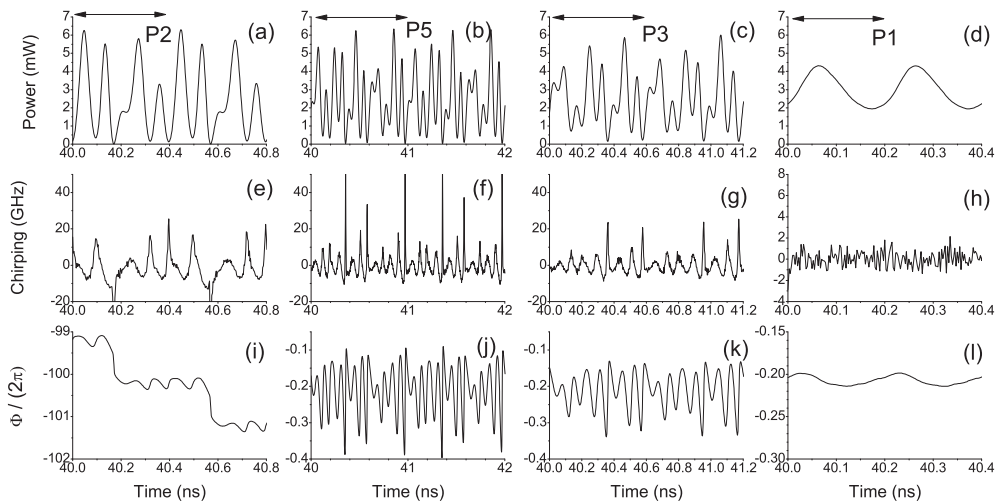


Fig. 9. Simulated power (upper row), chirping (middle row) and phase (lower row) of the gain-switched SL laser ( $I_{bias} = 30$  mA,  $f_R = 5$  GHz, and  $V_{RF} = 0.5$  V) with optical injection at detuning  $\Delta\nu_i = 4$  GHz and different values of injected power  $P_i$ , (a), (e), (i)  $250 \mu\text{W}$ , (b), (f), (j)  $338 \mu\text{W}$ , (c), (g), (k)  $416 \mu\text{W}$ , (d), (h), (l)  $2300 \mu\text{W}$ . In this figure  $\kappa_c = 1.5 \times 10^{11} \text{s}^{-1}$ .

Fig. 9(a), (e), and (i) illustrate the dynamics for the P2 regime corresponding to Fig 8(g). The period has been indicated with an horizontal arrow. Power and chirping traces show a clear repetition each  $2/f_R$ . Phase is locked because  $\Phi$  decreases  $2\pi$  each  $2/f_R$  in a similar way to the change of  $2\pi$  each  $1/f_R$  observed in Fig. 4(o). Our condition for phase locking goes beyond that of [42] because we consider that also a system with unbounded phase can be phase locked if the phase changes in  $2\pi$  after each period of the dynamics. Dynamics for P5 and P3 regimes, shown in the second and third column of Fig. 9, repeat each  $5/f_R$  and  $3/f_R$ , respectively. Phases are bounded and locked because they repeat with the previous periodicities, as seen in Fig. 9(j) and (k). This is

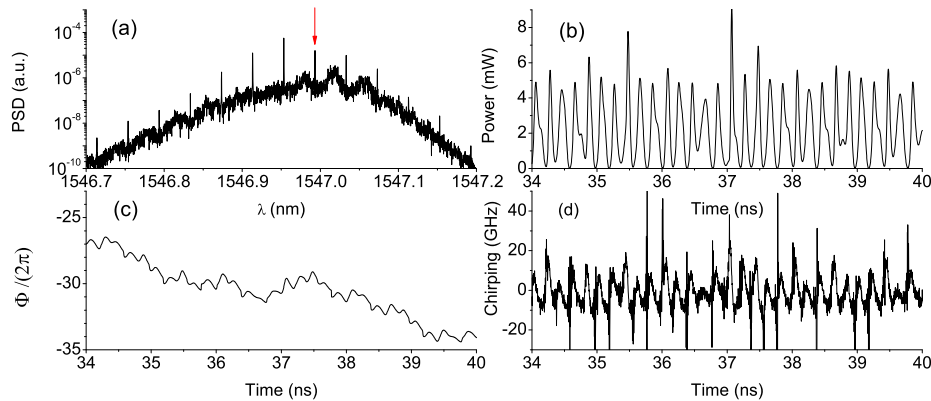


Fig. 10. Simulated (a) optical spectrum, and time traces of (b) power, (c) optical phase, and (d) frequency chirping at  $I_{bias} = 30$  mA,  $f_R = 5$  GHz,  $V_{RF} = 0.5$  V,  $\Delta\nu_i = -0.4$  GHz, and  $P_i = 20$   $\mu$ W. In this figure  $\kappa_c = 1.5 \times 10^{11}$  s $^{-1}$ . The wavelength of the optical injection is indicated with an arrow.

also the situation shown in the last column of Fig. 9 in which we illustrate that P1 is obtained when  $P_i$  is large enough, as obtained also experimentally.

We now illustrate the irregular dynamical behavior that appears in the maps of Figs. 6 and 7. Fig. 10 shows the simulated optical spectrum and the time traces corresponding to the highlighted point in the largest irregular region of Fig. 7. The optical spectrum features a broad pedestal on which comb lines separated by the repetition frequency  $f_R$  are still visible. Therefore, though the optical power emission is still pulsed with a repetition frequency  $f_R$ , the pulses are irregular in shape, height and width, as it is shown in Fig. 10(b). Fig. 10(c) shows the irregular and unbounded character of the optical phase. This behaviour is dominated by the deterministic evolution because the gain-switched SL is not completely switched-off between pulses (the minimum value of power in Fig. 10(b) is  $10^{-4}$  mW). Then the observed irregular dynamics can correspond to chaotic dynamics. In fact, we have checked that similar behavior is obtained when a much smaller value of  $\beta$  factor is considered ( $\beta = 10^{-12}$ ).

In the non-locking region we can find combs that are frequency-locked but do not fulfill the phase locking condition. These are for instance those obtained for low values of  $P_i$  when the MLs frequency becomes resonant with a rational fraction of  $f_R$ . One example is when light is injected at the middle of the two main tongues,  $\Delta\nu_i = -2.5$  GHz, and  $P_i = 50$  nW. The optical spectrum is similar to that of P2. However the dynamical state is not P2 because the phase is not locked. When plotted in the reference frame of the SL at CW operation the phase oscillates around a value performing a Brownian evolution, so it is not repeated after a  $2/f_R$  time.

Finally, we discuss the presence of multistability in our system. Multistability is characterized by the coexistence of several stable states for a fixed set of parameters. We have checked that a similar map to that of Fig. 6 is obtained when repeating the experiment in the same way. However, if we consider an alternative measurement method in which we fix  $P_i$  and change the ML frequency we observe that some dynamical regions appearing in Fig. 6 do not appear in the new measurements. These preliminar results seem to indicate that there is multistable behaviour in our system because there are differences between maps obtained by using different measurement procedures. Further investigations would be desirable to characterize multistability but they are outside the scope of this paper.

## 5. Conclusion

We have presented an experimental and theoretical study on the effect of optical injection on a high quality OFC generated by gain-switching a single-mode semiconductor laser. We have focused

on the nonlinear dynamics obtained when the bias current is modulated with a sinusoidal signal of  $f_R$  frequency. By using high-resolution optical spectra, we have measured two maps in which we have observed dynamics corresponding to injection-locked, unlocked and irregular combs. Injection-locked combs have been characterized in terms of their frequency and phase locking behavior. Several types of injection-locked combs have been obtained in which the frequency spacing between lines is equal to rational fractions of  $f_R$ . In the maps we have found different regions of locked combs with a tongue shape around detuning values given by multiples of  $f_R$ . An extended locking range for OFCs has been obtained when compared to CW lasers subject to optical injection. For large values of the modulation amplitude, locked regions mainly include combs with small values of the period, typically  $1/f_R$  or  $2/f_R$ . For smaller values of the modulation amplitude, the map is characterized by the appearance of many small-size locked regions with larger values of the period,  $N/f_R$ , with  $N > 2$  and up to 14. A very good agreement has been obtained between numerical simulations and experimental results. Our results have shown that optical frequency combs with different values of the frequency spacing can be obtained by using appropriate optical injection. PN dynamics can be useful for improving the resolution in dual-comb spectroscopy using gain-switched lasers while maintaining the large values of the spectral width obtained when  $f_R$  is close to the relaxation oscillation frequency.

## References

- [1] T. Fortier and E. Baumann, "20 years of developments in optical frequency comb technology and applications," *Commun. Phys.*, vol. 2, no. 1, pp. 1–16, 2019.
- [2] P. Trocha *et al.*, "Ultrafast optical ranging using microresonator soliton frequency combs," *Science*, vol. 359, no. 6378, pp. 887–891, 2018.
- [3] M. Imran, P. M. Anandarajah, A. Kaszubowska-Anandarajah, N. Sambo, and L. Poti, "A survey of optical carrier generation techniques for terabit capacity elastic optical network," *IEEE Commun. Surv. Tut.*, vol. 20, no. 1, pp. 211–263, Jan.–Mar. 2018.
- [4] J. Pfeifle *et al.*, "Flexible terabit/s nyquist-WDM super-channels using a gain-switched comb source," *Opt. Express*, vol. 23, pp. 724–738, 2015.
- [5] C. Browning *et al.*, "Gain-switched optical frequency combs for future mobile radio-over-fiber millimeter-wave systems," *J. Lightw. Technol.*, vol. 36, no. 19, pp. 4602–4610, Oct. 2018.
- [6] S. T. Cundiff and A. M. Weiner, "Optical arbitrary waveform generation," *Nature Photon.*, vol. 4, no. 11, pp. 760–766, 2010.
- [7] G. B. Rieker *et al.*, "Frequency-comb-based remote sensing of greenhouse gases over kilometer air paths," *Optica*, vol. 1, no. 5, pp. 290–298, 2014.
- [8] P. Martin-Mateos, M. Ruiz-Llata, J. Posada-Roman, and P. Acedo, "Dual-comb architecture for fast spectroscopic measurements and spectral characterization," *IEEE Photon. Technol. Lett.*, vol. 27, no. 12, pp. 1309–1312, Jun. 2015.
- [9] P.-T. Ho, L. Glasser, E. Ippen, and H. Haus, "Picosecond pulse generation with a CW gallium laser diode," *Appl. Phys. Lett.*, vol. 33, no. 3, pp. 241–242, 1978.
- [10] V. Torres-Company and A. M. Weiner, "Optical frequency comb technology for ultra-broadband radio-frequency photonics," *Laser Photon. Rev.*, vol. 8, no. 3, pp. 368–393, 2014.
- [11] J. Pfeifle *et al.*, "Coherent terabit communications with microresonator kerr frequency combs," *Nature Photon.*, vol. 8, no. 5, pp. 375–380, 2014.
- [12] P. Anandarajah *et al.*, "Generation of coherent multicarrier signals by gain switching of discrete mode lasers," *IEEE Photon. J.*, vol. 3, no. 1, Feb. 2011, Art. no. 5686909.
- [13] P. M. Anandarajah *et al.*, "Phase shift keyed systems based on a gain switched laser transmitter," *Opt. Express*, vol. 17, pp. 12 668–12 677, 2009.
- [14] V. Vujcic, P. M. Anandarajah, R. Zhou, C. Browning, and L. P. Barry, "Performance investigation of im/dd compatible ssb-ofdm systems based on optical multicarrier sources," *IEEE Photon. J.*, vol. 6, no. 5, Oct. 2014, Art. no. 7903110.
- [15] P. M. Anandarajah, S. P. Ó. Dúill, R. Zhou, and L. P. Barry, "Enhanced optical comb generation by gain-switching a single-mode semiconductor laser close to its relaxation oscillation frequency," *IEEE Jo. Sel. Topics Quantum Electron.*, vol. 21, no. 6, pp. 592–600, Dec. 2015.
- [16] S. P. Ó. Dúill, R. Zhou, P. M. Anandarajah, and L. P. Barry, "Analytical approach to assess the impact of pulse-to-pulse phase coherence of optical frequency combs," *IEEE J. Quantum Electron.*, vol. 51, no. 11, Nov. 2015, Art. no. 1200208.
- [17] S. P. Ó. Dúill, P. M. Anandarajah, R. Zhou, and L. P. Barry, "Numerical investigation into the injection-locking phenomena of gain switched lasers for optical frequency comb generation," *Appl. Phys. Lett.*, vol. 106, no. 21, 2015, Art. no. 211105.
- [18] A. R. Criado, C. de Dios, E. Prior, M. Ortsiefer, P. Meissner, and P. Acedo, "VCSEL-based optical frequency combs: Toward efficient single-device comb generation," *IEEE Photon. Technol. Lett.*, vol. 25, no. 20, pp. 1981–1984, Oct. 2013.
- [19] E. Prior, C. De Dios, M. Ortsiefer, P. Meissner, and P. Acedo, "Understanding VCSEL-based gain switching optical frequency combs: Experimental study of polarization dynamics," *J. Lightw. Technol.*, vol. 33, no. 22, pp. 4572–4579, Nov. 2015.

- [20] B. Jerez, P. Martin-Mateos, E. Prior, C. de Dios, and P. Acedo, "Dual optical frequency comb architecture with capabilities from visible to mid-infrared," *Opt. Express*, vol. 24, pp. 14986–14994, 2016.
- [21] S. Chandran, S. Mahon, A. A. Ruth, J. Braddell, and M. D. Gutierrez, "Cavity-enhanced absorption detection of H<sub>2</sub>S in the near-infrared using a gain-switched frequency comb laser," *Appl. Phys. B*, vol. 124, pp. 63–71, 2018.
- [22] A. Rosado, A. Pérez-Serrano, J. M. G. Tijero, A. Valle, L. Pesquera, and I. Esquivias, "Experimental study of optical frequency comb generation in gain-switched semiconductor lasers," *Opt. Laser Technol.*, vol. 108, pp. 542–550, 2018.
- [23] A. Rosado, A. Pérez-Serrano, J. M. G. Tijero, A. Valle, L. Pesquera, and I. Esquivias, "Enhanced optical frequency comb generation by pulsed gain-switching of optically injected semiconductor lasers," *Opt. Express*, vol. 27, pp. 9155–9163, 2019.
- [24] A. Rosado, A. Pérez-Serrano, J. M. G. Tijero, A. Valle, L. Pesquera, and I. Esquivias, "Numerical and experimental analysis of optical frequency comb generation in gain-switched semiconductor lasers," *IEEE J. Quantum Electron.*, vol. 55, no. 6, Dec. 2019, Art. no. 2001012.
- [25] F. A. Gutiérrez, E. P. Martin, P. Perry, A. D. Ellis, P. M. Anandarajah, and L. P. Barry, "WDM orthogonal subcarrier multiplexing," *J. Lightw. Technol.*, vol. 34, no. 8, pp. 1815–1823, Jul. 2015.
- [26] A. R. Criado *et al.*, "Continuous-wave sub-THz photonic generation with ultra-narrow linewidth, ultra-high resolution, full frequency range coverage and high long-term frequency stability," *IEEE Trans. THz Sci. Technol.*, vol. 3, no. 4, pp. 461–471, Jul. 2013.
- [27] R. Zhou, T. N. Huynh, V. Vujicic, P. M. Anandarajah, and L. P. Barry, "Phase noise analysis of injected gain switched comb source for coherent communications," *Opt. Express*, vol. 22, no. 7, pp. 8120–8125, 2014.
- [28] M. D. G. Pascual, R. Zhou, F. Smyth, P. M. Anandarajah, and L. P. Barry, "Software reconfigurable highly flexible gain switched optical frequency comb source," *Opt. Express*, vol. 23, no. 18, pp. 23 225–23 235, 2015.
- [29] R. Lang, "Injection locking properties of a semiconductor laser," *IEEE J. Quantum Electron.*, vol. 18, no. 6, pp. 976–983, Jun. 1982.
- [30] S. Wieczorek, B. Krauskopf, T. B. Simpson, and D. Lenstra, "The dynamical complexity of optically injected semiconductor lasers," *Phys. Rep.*, vol. 416, pp. 1–128, 2005.
- [31] K. Shortiss, B. Lingnau, F. Dubois, B. Kelleher, and F. H. Peters, "Harmonic frequency locking and tuning of comb frequency spacing through optical injection," *Opt. Express*, vol. 27, no. 25, pp. 36 976–36 989, 2019.
- [32] B. Lingnau, K. Shortiss, F. Dubois, B. Kelleher, and F. H. Peters, "The devil's staircase in the frequency and amplitude locking of nonlinear oscillators with continuous periodic forcing," 2019, *arXiv:1905.01122*.
- [33] A. Gavrielides, "Comb injection and sidebands suppression," *IEEE J. Quantum Electron.*, vol. 50, no. 5, pp. 364–371, May 2014.
- [34] L. Fan *et al.*, "Generation of tunable and ultra-broadband microwave frequency combs based on a semiconductor laser subject to pulse injection from a current modulated laser," *IEEE Photon. J.*, vol. 10, no. 6, Dec. 2018, Art. no. 5502310.
- [35] Y. Doumbia, T. Malica, D. Wolfersberger, K. Panajotov, and M. Sciamanna, "Optical injection dynamics of frequency combs," *Opt. Lett.*, vol. 45, no. 2, pp. 435–438, 2020.
- [36] H. Zhu, R. Wang, T. Pu, P. Xiang, J. Zheng, and T. Fang, "A novel approach for generating flat optical frequency comb based on externally injected gain-switching distributed feedback semiconductor laser," *Laser Phys. Lett.*, vol. 14, no. 2, 2016, Art. no. 026201.
- [37] L. Fan *et al.*, "Tunable ultra-broadband microwave frequency combs generation based on a current modulated semiconductor laser under optical injection," *IEEE Access*, vol. 5, pp. 17 764–17 771, 2017.
- [38] P. Anandarajah *et al.*, "Discrete mode lasers for communication applications," *IET Optoelectron.*, vol. 3, pp. 1–17, 2009.
- [39] N. Schunk and K. Petermann, "Noise analysis of injection-locked semiconductor injection lasers," *IEEE J. Quantum Electron.*, vol. 22, no. 5, pp. 642–650, May 1986.
- [40] S. Mohrdiek, H. Burkhard, and H. Walter, "Chirp reduction of directly modulated semiconductor lasers at 10 Gb/s by strong CW light injection," *J. Lightw. Technol.*, vol. 12, no. 3, pp. 418–424, Mar. 1994.
- [41] H.F. Liu, and W.F. Ngai, "Nonlinear dynamics of a directly modulated 1.55  $\mu\text{m}$  InGaAsP distributed feedback semiconductor laser," *IEEE J. Quantum Electron.*, vol. 29, no. 6, pp. 1668–1675, Jun. 1993.
- [42] J. Thevenin, M. Romanelli, M. Vallet, M. Brunel, and T. Erneux, "Resonance assisted synchronization of coupled oscillators: Frequency locking without phase locking," *Phys. Rev. Lett.*, vol. 107, 2011, Art. no. 104101.